

Turbulent Diffusion in the Photosphere as Derived from Photospheric Bright Point Motion

Abramenko, V.I.¹, Carbone, V.², Yurchyshyn, V.¹, Goode, P.R.¹, Stein, R.F.³, Lepreti,
F.², Capparelli, V.², Vecchio, A.²

¹ Big Bear Solar Observatory, 40386 N. Shore Lane, Big Bear City, CA 92314, USA;

² Dipartimento di Fisica, Universita della Calabria- Via P. Bucci 31/C, I-87036 Rende,
Italy;

³ Department of Physics & Astronomy, Michigan State University, East Lansing, MI 48824,
USA

ABSTRACT

On the basis of observations of solar granulation obtained with the New Solar Telescope (NST) of Big Bear Solar Observatory, we explored proper motion of bright points (BPs) in a quiet sun area, a coronal hole, and an active region plage. We automatically detected and traced bright points (BPs) and derived their mean-squared displacements as a function of time (starting from the appearance of each BP) for all available time intervals. In all three magnetic environments, we found the presence of a super-diffusion regime, which is the most pronounced inside the time interval of 10-300 seconds. Super-diffusion, measured via the spectral index, γ , which is the slope of the mean-squared displacement spectrum, increases from the plage area ($\gamma = 1.48$) to the quiet sun area ($\gamma = 1.53$) to the coronal hole ($\gamma = 1.67$). We also found that the coefficient of turbulent diffusion changes in direct proportion to both temporal and spatial scales. For the minimum spatial scale (22 km) and minimum time scale (10 sec), it is 22 and 19 km² s⁻¹ for the coronal hole and the quiet sun area, respectively, whereas for the plage area it is about 12 km² s⁻¹ for the minimum time scale of 15 seconds. We applied our BP tracking code to 3D MHD model data of solar convection (Stein et al. 2007) and found the super-diffusion with $\gamma = 1.45$. An expression for the turbulent diffusion coefficient as a function of scales and γ is obtained.

Subject headings: Sun: photosphere; surface magnetism. Physical Data and Processes: turbulence

1. Introduction

Diffusion of magnetic elements on the solar surface reflects sub-photospheric turbulent convection. It is an energy source for heating upper layers of the solar atmosphere and is essential for dynamo action. These circumstances justify the persistent interest of scientists to various problems related to turbulent diffusion of solar magnetic fields.

Recent observations of the solar magnetic surface with high powered space- and ground-based instruments demonstrated, beyond doubt, that the quiet sun (QS) magnetic fields can no longer be considered to be sheets of unipolar magnetic flux stretching along the boundaries of supergranules. Hinode instruments (Kosugi et al. 2007; Tsuneta et al. 2008) facilitated a significant breakthrough in our understanding of QS magnetism: Ubiquitous transverse magnetic fields (e.g., Lites et al. 2008; Ishikawa et al. 2010; Ishikawa & Tsuneta 2010) and fine intranetwork mixed polarity fields (e.g., de Wijn et al. 2008, 2009) were discovered. The launch of the IMaX spectropolarimeter on-board the Sunrise balloon-borne solar observatory (Martinez Pillet et al. 2011) allowed one the resolution of individual kG flux (Lagg et al. 2010) and exploration of vortex flow motions (Bonet et al. 2010), to mention a few (for more results from IMaX/Sunrise experiment see a special issue of The Astrophysical Journal Letters, 713).

All of this new information suggests that the QS magnetic fields can not be fully explained as remnants of decaying active regions but rather leads to the idea that an additional mechanism for magnetic field generation, such as local turbulent dynamos (see review by Petrovay 2001, Pietarila Graham et al. 2010, and references herein), should be at work. One of the essential parameters for generating magnetic fields via turbulent dynamo action is the magnitude of magnetic diffusivity: in the case of very high diffusivity, chances for magnetic field concentrations to resist the spreading action of turbulent flows are small and, so, the dynamo could be restrained.

Another important question is how diffusivity varies with spatial and time scales? The commonly accepted mechanism that transports magnetic flux over the solar surface is random walk, or, *normal diffusion*, when the mean-squared displacements of flow tracers vary with time, τ , as $\langle(\Delta l)^2\rangle = 4K\tau \sim \tau^\gamma$, where K is the diffusion coefficient (a scalar), and $\gamma = 1$. In this case diffusivity does not vary with spatial and temporal scales. Generally, when index γ deviates from unity, the diffusion is then called *anomalous*. More specifically, the regime with $\gamma > 1$ is called *super-diffusion* (the diffusion coefficient grows with scales), while $\gamma < 1$ indicates *sub-diffusion* (the diffusion coefficient decreases when the scales increase, see Section 6).

From tracking magnetic elements, Lawrence & Schrijver (1993) reported an anomalous

sub-diffusion on supergranular spatial scales and time scales of days. They found the diffusivity spectral index $\gamma = 0.89 \pm 0.20$, which is smaller than unity and thus implies sub-diffusion. Cadavid et al. (1999) tracked G-band bright points and found sub-diffusivity ($\gamma = 0.76 \pm 0.04$) on granular scales and time intervals of 0.3-22 minutes and nearly normal diffusion ($\gamma = 1.10 \pm 0.24$) for 25-57 minutes. Later, Lawrence et al. (2001), utilized the same G-band data set by applying subsonic filtering (i.e., removing displacements with velocities larger than 7 km s^{-1} - the photospheric sound speed), and they reported super-diffusion with $\gamma = 1.27 \pm 0.01$ on time scales of 0.8-34 minutes. They also found that in the frameworks of the continuous time random walk approach (CTRW, see, e.g., Campos & Mendez 2008; Zoia et al. 2010, see also references in Cadavid et al. 1999), the diffusion exponent is 1.54 ± 0.39

Above we discussed studies that explored the regime of anomalous diffusion only, whereas a voluminous body of literature exists that deals with derivation of diffusivity coefficient in the framework of normal diffusion.

For example, Hagenaar et al. (1999) analyzed displacements of magnetic elements and found that the magnetic diffusion coefficient also depend on the time scale: it is about $70\text{-}90 \text{ km}^2\text{s}^{-1}$ when measured over time intervals of 1-3 hours and it increases to $200\text{-}250 \text{ km}^2\text{s}^{-1}$ for time intervals longer than 8 hours. Berger et al. (1998b) tracked G-band BPs observed with the Swedish Vacuum Solar Telescope (SVST) and found a decreasing diffusion coefficient for time scales growing from 23 sec to approximately 25 min, while there was a slight increase for longer time scales (from 50 to $79 \text{ km}^2\text{s}^{-1}$ on time scales from 27 to 57 minutes).

Chae et al. (2008) reported an increase in the diffusion coefficient as the smallest resolved spatial scale increases. A review of the photospheric magnetic diffusion covering the pre-Hinode era is given in Schrijver et al. (1996), where the authors emphasize a significant discrepancy between the previously reported diffusivity values. The reasons for that seem to be an acute sensitivity of the derived values to the temporal and spatial resolution of data, as well as the intrinsic dependence of the rate of turbulent diffusion on the spatial scale (see, e.g., Monin & Yaglom 1975; Chae et al. 2008).

In the present study, we focus on properties of magnetic diffusion in the quiet sun photosphere, especially on their changes with varying temporal and spatial scales. Bright features, visible in the dark inter-granule lanes, are called bright points (BPs) and they are thought to be footpoints of magnetic flux tubes (e.g., Muller et al. 2000; Berger & Title 2001; Ishikawa et al. 2007, to mention a few). Therefore, they make it possible for us to measure the dynamics of the photospheric magnetic flux tubes. Only a fraction (about 20%, de Wijn et al. 2008) of magnetic elements are thought to be associated with BPs,

therefore they allow us to study only a subset of the entire magnetic flux tube population. For that purpose, we will use the highest resolution data on solar granulation (see Table 1) obtained with the New Solar Telescope (NST, Goode et al. 2010a) of the Big Bear Solar Observatory (BBSO).

Table 1: Parameters of Solar Instruments

Name	D, cm	λ , nm	Diff limit	Pixel	Cadence, s	AO ^a	Speckle	Reference
SOHO/MDI/HR	10	676.7	1.''70	0.''6	60	NO	NO	Sherrer et al. 1995
SDO/HMI	14	617.3	1.''11	0.''5	45	NO	NO	http://hmi.stanford.edu/
Hinode/SOT	50	430.5	0.''216	0.''109	60	NO	NO	Tsuneta et al. 2008
		630.2	0.''316	0.''16	120	NO	NO	Tsuneta et al. 2008
SVST	50	430.5	0.''216	0.''083	23	NO	NO	Berger et al. 1998b
SST	100	430.5	0.''108	0.''041	20	YES	YES	Scharmer et al. 2003
DST/ROSA	76	430.5	0.''142	0.''069	23	YES	YES	Crockett et al. 2010
IMaX/SUNRISE	100	525.0	0.''132	0.''055	33	NO	NO	Barthol et al. 2011
BBSO/NST	160	705.7	0.''110	0.''0375	10	YES	YES	Goode et al. 2010b

^a – adaptive optics correction.

2. Data and Analysis

In this study, we analyzed three different data sets: i) a quiet sun internetwork/network area (QS), ii) a coronal hole area (CH), and iii) a plage area inside an active region (ARP).

Solar granulation was observed with the NST, which is a 1.6 meter clear aperture off-axis reflector (Goode et al. 2010a,b). The observations were taken with a 1 nm bandpass TiO interference filter centered at a wavelength of 705.7 nm. Previously, photospheric BPs were studied with G-band data (e.g., Berger et al. 1998a,b; Cadavid et al. 1999; Utz et al. 2009, 2010; Crockett et al. 2010; Sanchez Almeida et al. 2010, to mention a few) obtained using an interference filter centered at 430.5 nm. Direct comparison of simultaneous Hinode G-band and NST/TiO images of the same area (see Figure 1 in Abramenko et al. 2010) showed that although there is a difference in BP intensities, these two spectral ranges are equally suitable for detecting photospheric BPs.

The QS data set was obtained during an uninterrupted observing run between 17:06 and 18:57 UT on August 3, 2010, when the telescope was pointed at the disk center and seeing conditions were excellent. A total of 648 images with a 10 second cadence were obtained. The CH data set consists of 183 images taken with a 15 second cadence obtained on August 31, 2010 between 17:41 UT and 18:15 UT. The telescope was pointed at a

confined CH located at E12N02. The ARP data set has 513 images with a 10 second cadence of AR NOAA 11109 recorded on September 27, 2010 between 17:22 UT and 19:51 UT. The CH and ARP sets were both recorded at very good seeing conditions. All data sets were adaptive optics (AO) corrected, speckle reconstructed and destretched.

To produce one speckle reconstructed image, we need bursts of images taken in a rapid succession. The KISIP speckle reconstruction code (Woger et al. 2008) was applied to each burst consisting of 70 images taken with a 1 ms exposure. All reconstructed (final) images were aligned and de-stretched. A subsonic filter with a $v < 7 \text{ km s}^{-1}$ cut-off was applied to each final image to remove acoustic and f -mode oscillations (Title et al. 1989). Typical final data images are shown in Figure 1. A movie of the QS data set can be found at the BBSO website ¹.

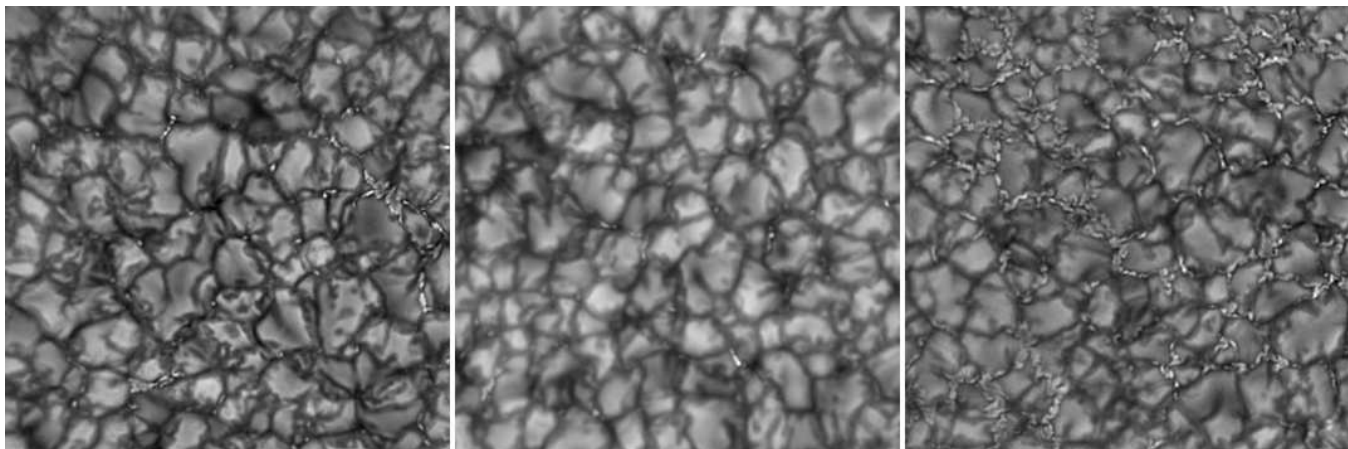


Fig. 1.— Samples of TiO data for QS (left), CH area (middle) and AR plage area (right). The FOV of each frame is $22'' \times 22''$ or 590×590 pixels.

BPs were automatically detected in all images and then tracked from one image to the next. Here we used the detection and tracking code previously described in Abramenko et al. (2010). In general, our method uses the same approach as that of Berger et al. (1998a,b), i.e., BPs are first enhanced in the images (by subtracting a smoothed copy of the same image) and then selected by applying thresholding and masking.

Typical examples of trajectories of BPs derived from the QS set are plotted in Figure 2. They show that gradual drift of a BP is intermittent, punctuated with rapid displacements. To clarify the possible reasons for these rapid shifts, we estimated the residual image jittering in the data set by computing an offset of each image relative to the previous image

¹http://bbsso.njit.edu/nst_gallery.html

using a Fourier aligning procedure. In Figure 3, we separately plot x and y coordinates of the trajectory shown in the right panel of Figure 2 along with the corresponding residual x - and y -offsets. The figure shows (and the calculations of the corresponding correlation coefficient confirm) that the rapid displacements of BPs are not due to poor image alignment: image jittering is very small and stable with the r.m.s. value of 0.1 pixel (2.7 km) and the maximum value of 0.26 pixel. We therefore adopt an r.m.s. value of 2.7 km as a typical error of calculations of the BP position.

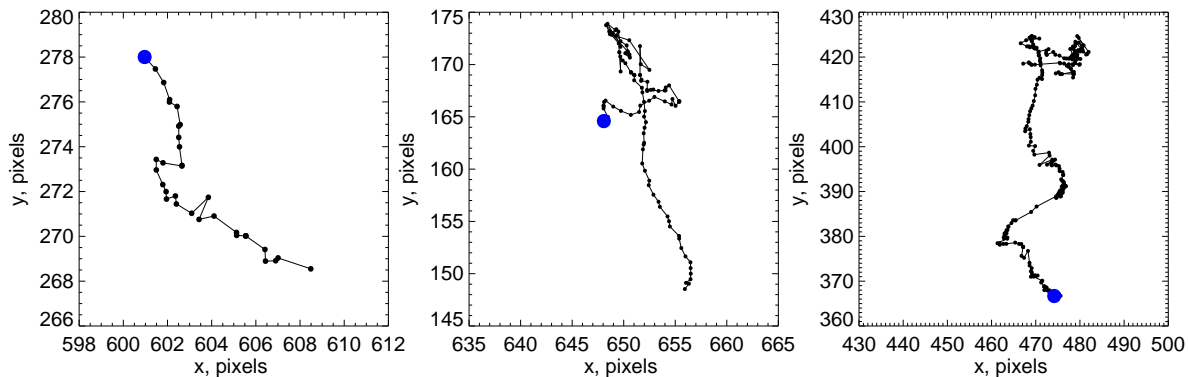


Fig. 2.— Typical trajectories of BPs. The time intervals between adjacent measurements (circles) is 10 seconds. Blue circles mark the start point of the trajectory.

In Figure 4, the first image in the QS data set is overplotted with all derived BP trajectories. The BP tracks do not evenly cover the FOV (or solar surface, for that matter) instead, they rather tend to lie along the supergranular boundaries, i.e., along the network of magnetic fields. This picture qualitatively agrees with previous studies (Lawrence & Schrijver 1993; Cadavid et al. 1999). Namely, Lawrence & Schrijver (1993) reported the fractal dimension of a set of random walk sites to be $D = 1.56 \pm 0.08$. In our case, the fractal dimension of the red-colored area in Figure 4 is slightly lower, 1.45 ± 0.06

3. Lagrangian Velocities

A traditional method to describe turbulence is the Euler approach, when one studies statistical properties of a flow by analyzing a velocity field specified at all spatial points of the volume. This method is useful, especially in modeling of turbulent flows. However, when we are dealing with diffusive properties of tracers within a turbulent fluid flows, the Lagrangian approach is more efficient than (see, e.g., Monin & Yaglom 1975). It is based

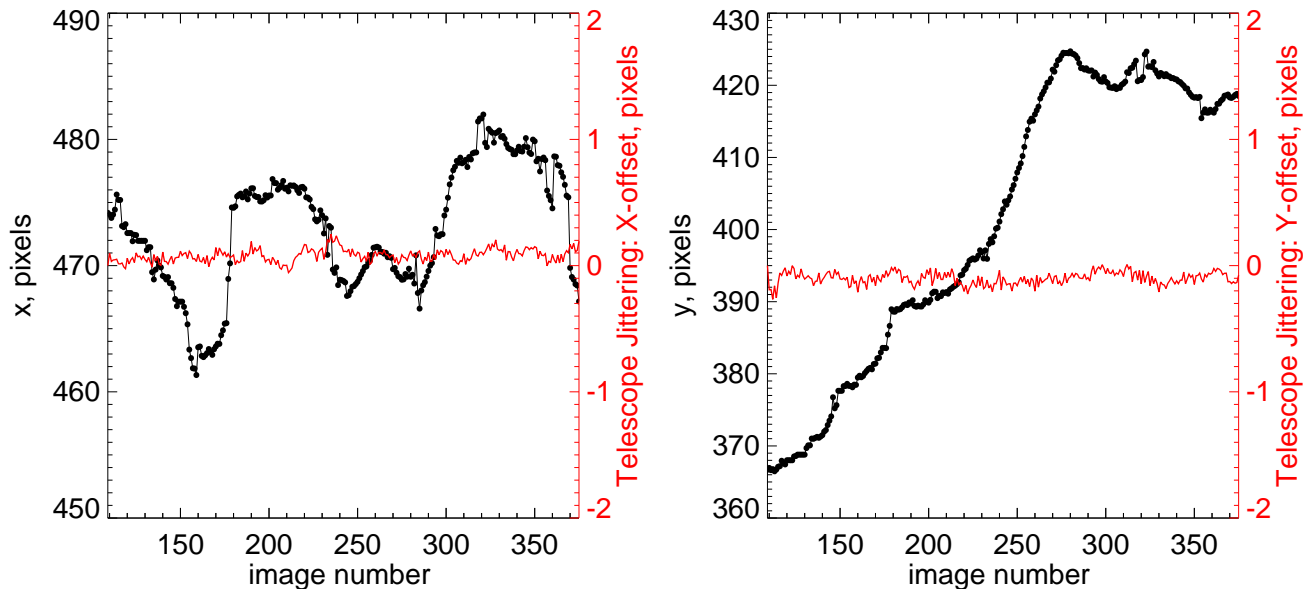


Fig. 3.— x and y coordinates of the BP shown in the right panel of Figure 2, overplotted with co-temporal variations of the offset between two consecutive images (red lines, right axes). Note the scale difference between BP’s displacements (left axes) and the residual image offset (right axes).

on description of statistical properties of an individual “fluid particle” embedded in the turbulent flow. Such particles are assumed to be large enough, compared to the molecular scale, and, at the same time, small enough to be considered as solid bodies shifted as a whole (without inner deformation). The Lagrangian approach is directly related to the real motions of the physical particles that form the turbulent flow, and as such, it is more realistic, as compared to the Euler method.

Photospheric BPs seem to be good candidates for such “fluid particles” that are transported by turbulent photospheric flows. This approach was used, for example, by van Ballegoijen et al. (1998) to determine the Lagrangian velocity correlation function with subsequent application to the coronal heating problem (Cranmer & van Ballegoijen 2005). Here we utilize the Lagrangian method to examine the turbulent diffusion in the quiet Sun photosphere.

Our first step was to compute the spatial displacement, $(\Delta l)_i$, of an individual i -th BP as a function of time interval, τ , measured in seconds from the moment of the first detection of this BP. We then calculated the average (over all BPs) displacement for each time

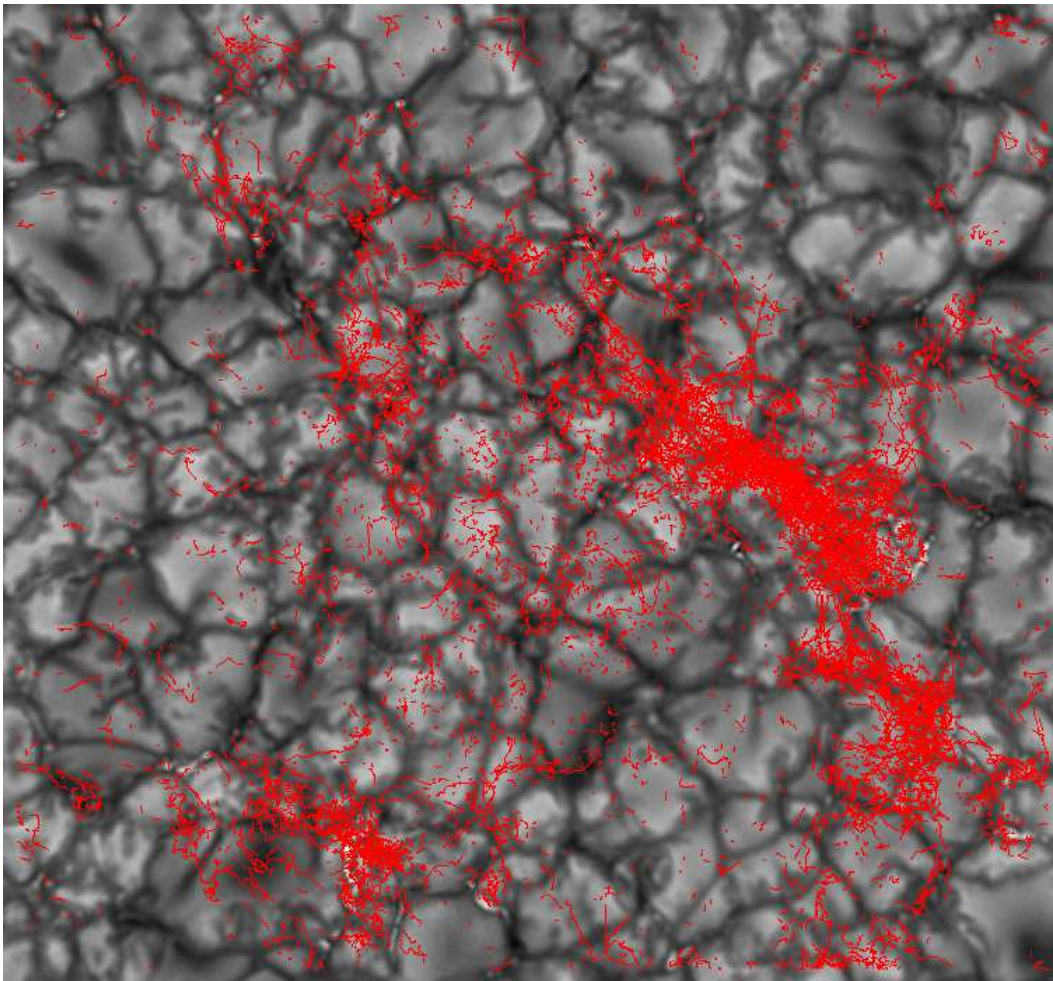


Fig. 4.— Trajectories (red) of all BPs detected from the QS data set and persisted longer than 3 timesteps. Background is the first image of the data set.

interval to obtain the average squared displacement as a function of time (the displacement spectrum).

$$(\Delta l)^2(\tau) = \langle |\mathbf{X}_i(0) - \mathbf{X}_i(\tau)|^2 \rangle, \quad (1)$$

where $\mathbf{X}_i(0) = (x_0, y_0)$ and $\mathbf{X}_i(\tau) = (x_\tau, y_\tau)$ are coordinates of the i -th BP at the moment of its first detection and τ seconds later, respectively. The form of the function $(\Delta l)^2(\tau)$ is the key for understanding the nature of the turbulent diffusion. The power index, γ , of the displacement spectrum is defined as

$$(\Delta l)^2(\tau) \sim \tau^\gamma \quad (2)$$

and in practice is derived as a slope of the spectra over a range of τ . This index was used to quantify the strength of diffusivity (see, e.g., Cadavid et al. 1999).

A broad definition of γ for various statistical moments was discussed and applied for solar data by Lawrence et al. (2001). Here we utilize only the second statistical moment of displacements.

4. Diffusion Regime in the Photosphere as Derived from Various Sources

To understand how our results could be affected by the resolution of the data and its quality, we performed the following tests. First, using the QS data set, we calculated $(\Delta l)^2(\tau)$ in four different ways. Results are shown in Figure 5. There, the black dots and black solid straight line represent results for 7912 BPs derived from the final QS data set as described in the Data section: i.e., speckle reconstructed, aligned, de-stretched, subsonic-filtered images with 10 seconds time cadence utilized to detect BPs with an area of no less than 3 squared pixels, that lasted more than 3 time steps. The power law index, γ , calculated as the best linear fit to the data points within the 10-300 s time interval, was found to be 1.530 ± 0.005 .

Next, we degraded the data set by applying a 3-point running-box averaging along the time axis (green circles and lines in Figure 5), thus essentially eliminating the inhomogeneity of the intensity distribution (important to determine the location and the center of a BP). We thus detected total 6661 events and the power law index in this case increased only slightly relative to the un-degraded original data (from 1.53 to 1.60).

We repeated the same calculations taking into account only large, bright and long living BPs (red color symbols and line in Figure 5). The BP area threshold was set here to 8 pixels, the life time threshold to 10 time steps (100 s), and the brightness threshold to 90 DN (instead of 85 DN). Under these requirements, we detected only 1861 tracked BPs. In this test run, all possible uncertainties arising from analyzing low intensity, small, short living BPs (which actually comprise the majority of the detected BPs) were eliminated. The results, however, were not much different: the power index, γ , determined within the same time interval of 10-300 s was 1.538 ± 0.010 . At larger time scales (above approximately 700 s), the difference with the previous experiments is more noticeable, but still negligible.

In our final experiment (blue color data points in Figure 5), we first re-binned the original QS data set to the 2×2 original pixels mesh, and then convolved it with a Gaussian function to mimic $0.''4$ spatial resolution. Afterward, we discarded every even image in the data set to increase the time cadence to 20 s. In doing so, we degraded the resolution and

time cadence of our data set to closely match that utilized in Cadavid et al. (1999). The intensity threshold for BP detection was set to 105 DN, so that only brightest BPs were taken into account. The total number of detected tracked BPs was only 840. The blue line in Figure 5 that corresponds to this experiment, is the lowest one, which means that on average the displacements are smaller. However, the power index $\gamma = 1.544 \pm 0.010$, which is very similar to the value of $\gamma = 1.530 \pm 0.005$ inferred from the un-degraded original data set.

Subsonic filtering did not significantly affect our results, we obtained $\gamma = 1.535 \pm 0.008$ for the non-filtered QS data set.

The above exercise shows that index γ determined for small time scales (< 300 s) does not seem to depend on data processing and apparently reflects an intrinsic property of BP's motions recorded in the data set: a super-diffusion turbulent regime with $\gamma \approx 1.5$. Only on larger time scales (> 600 s), the function $(\Delta l)^2(\tau)$ depends slightly on data processing and/or spatial resolution.

Another reason for the discrepancies may be that the NST data enable us to measure much smaller BP displacements than the SVST observations do. To explore this possibility, we discarded all squared displacements $(\Delta l)^2(\tau)$ smaller than the SVST squared displacement detection threshold, 3500 km^2 (see Fig. 1 in Cadavid et al. 1999). The result is shown in Figure 6 (crosses). At small scales ($\tau < 200$ s), data points are well above the original data points (red). Interestingly, for the time scales of 40-300 s, the slope of the spectrum is 1.26 ± 0.02 , which is very close to that reported by Lawrence et al. (2001) from the SVST data.

Two additional tests described below further confirm validity of super-diffusion regime and the relevance of data quality for measuring the index, γ , of the displacement spectra.

First, we applied our code to model data of solar granulation obtained from 3D MHD solar magneto-convection simulations (Stein et al. 2007). The model data set consisted of 146 intensity images of 1008×1008 pixels (48×48 Mm) separated by a 60 s time intervals. Three fragments of the simulated intensity images are shown in Figure 7. The surface density of BPs in this case was lower than that for the observed QS data. The model data show super-diffusion with $\gamma = 1.451 \pm 0.061$ inside the time interval of 60 - 660 s (Figure 6, green symbols), which is in good agreement with observations.

In the second run, we applied our code to an NST data set obtained on July 29, 2009 (see Goode et al. 2010b for description of this data set). The main reason to use this set is that it is of inferior quality as compared to the August 3, 2010 data utilized in this study. In particular, the July 29, 2009 data were recorded under good seeing conditions

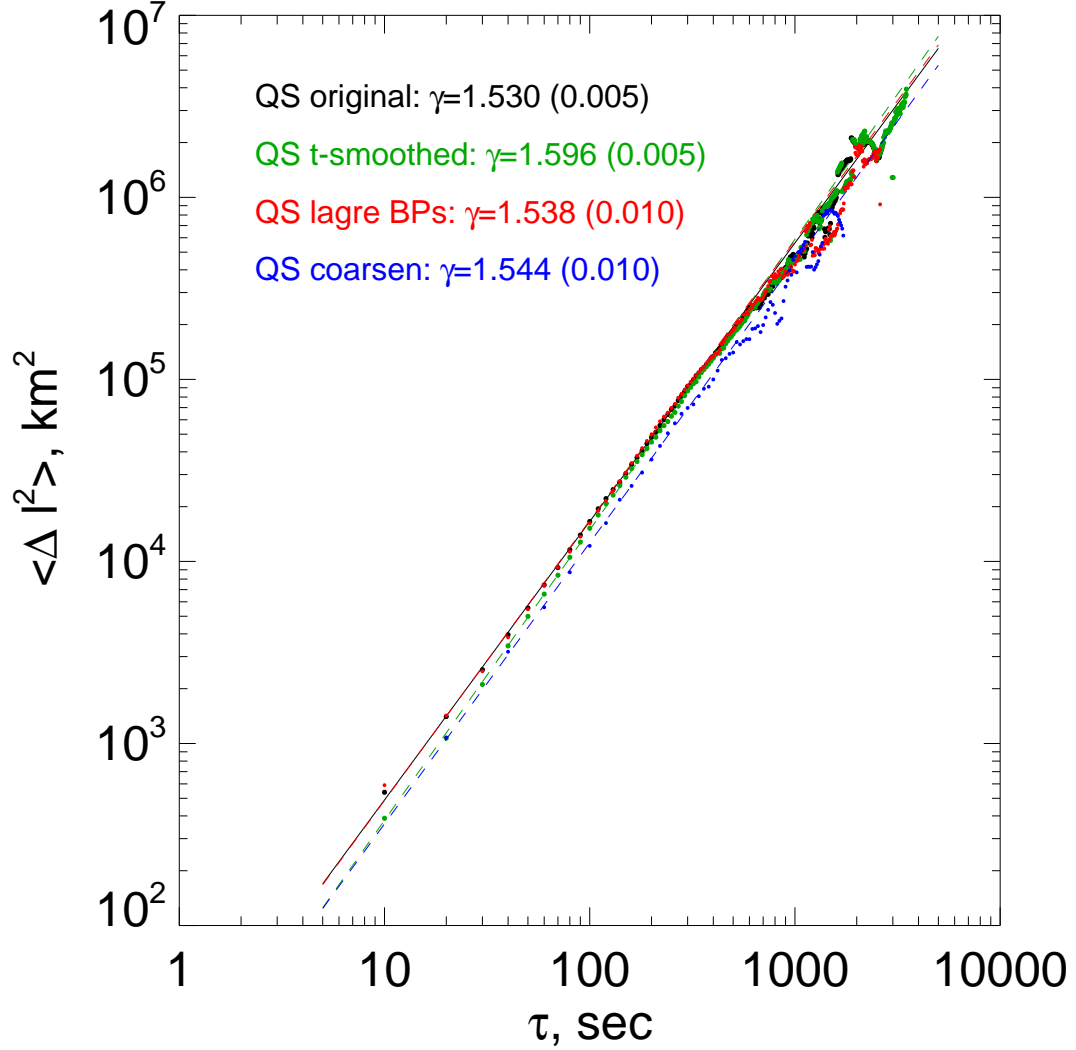


Fig. 5.— Displacements $(\Delta l)^2(\tau)$ computed according to Eq. 1. Black data symbols represent results derived from the original QS data set, green colors represent results derived from the time-smoothed data set, red colors are plot results derived from a subset of only large, bright and long-live BPs, while blue symbols represent the result for the most degraded version of the data set (2×2 re-binned and Gaussian-deconvolved data set of 20 s cadence). In all cases, the error bars did not exceed the size of the plotting symbols. In all experiments, slope γ was calculated as the best linear fit inside the range of 10-300 s. One- σ errors of the fitting are shown in brackets.

without the AO correction, and the time coverage was four times shorter. The displacement spectrum obtained from these inferior data (Figure 6, blue symbols) has poorer linearity,

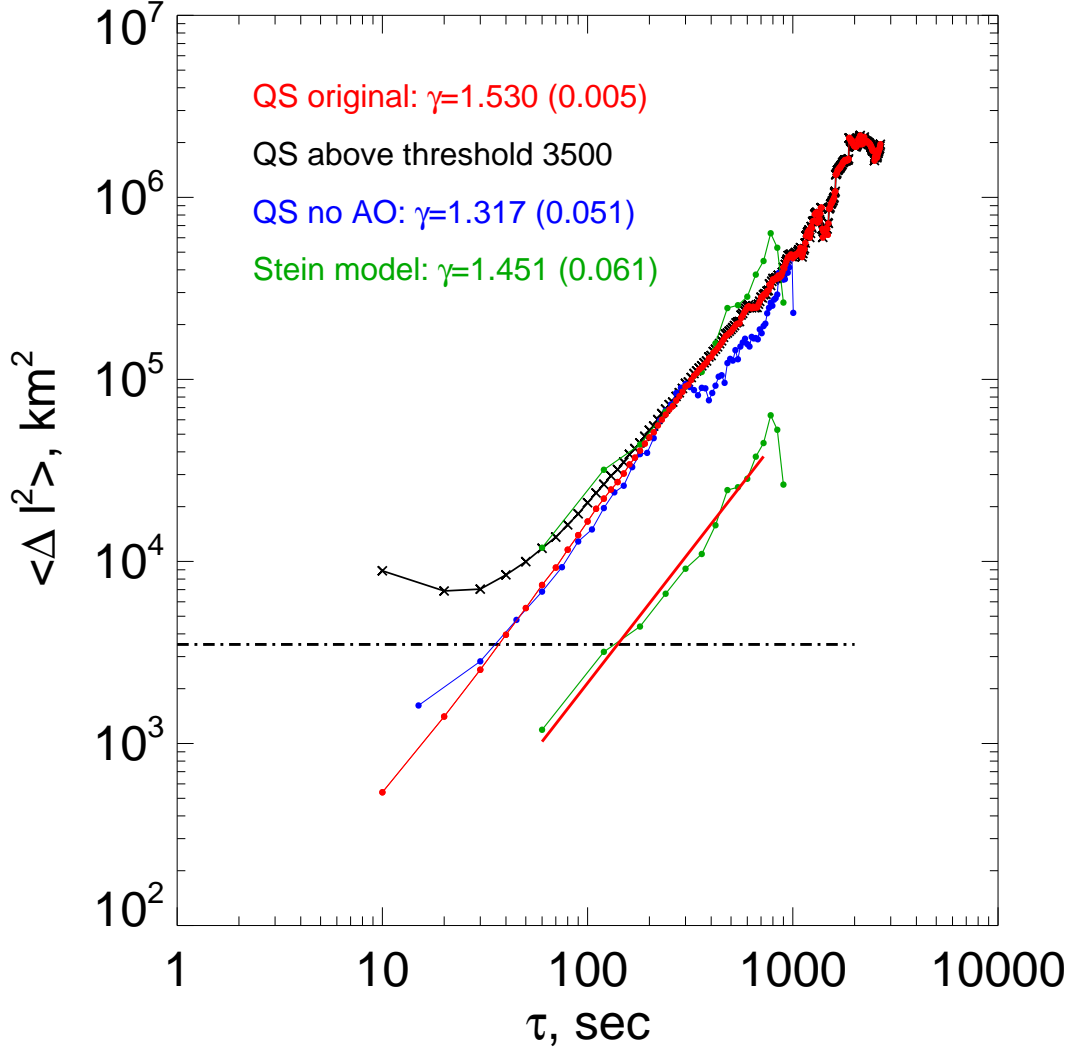


Fig. 6.— Function $\langle \Delta l^2 \rangle(\tau)$ derived from i) the original QS data set (red), ii) small displacements (below a 3500 km² threshold, black dash-dotted line) in the original QS data set were discarded (crosses); iii) July 29, 2009 NST data set recorded without an AO correction (blue), and iv) model solar granulation data (green, Stein et al. 2007). For better viewing, the model data are also shifted down and their best linear fit is shown with the thick red straight line.

less pronounced super-diffusion regime and narrower range of super-diffusion. The spectral index γ is equal to 1.317 ± 0.051 inside the time interval of 15 - 210 s.

All the tests performed in this section point to a conclusion that spatial and temporal

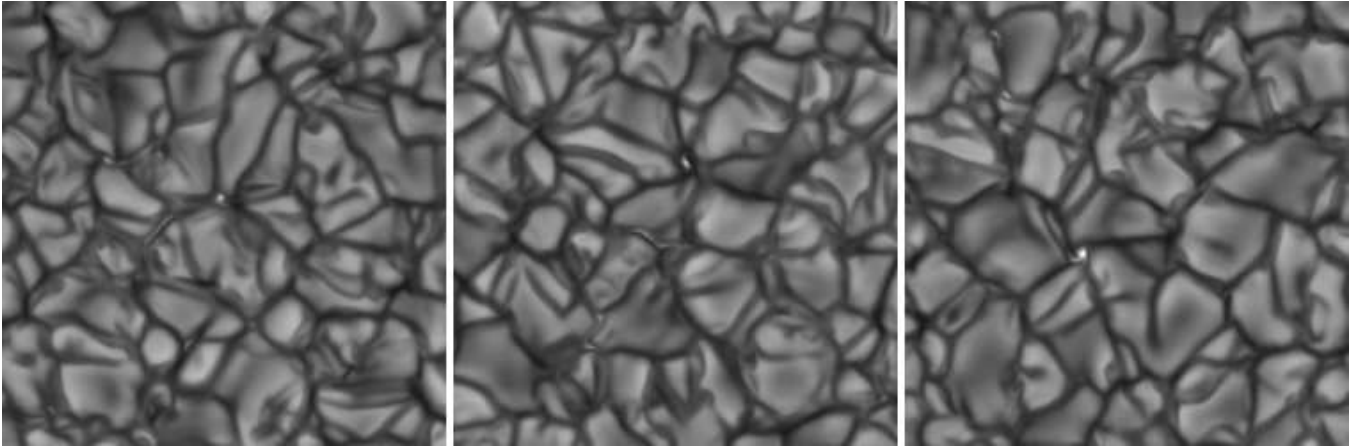


Fig. 7.— Three fragments of simulated solar granulation images obtained from a 3D MHD solar magneto-convection code (Stein et al. 2007). BPs in intergranular lanes are visible.

resolution affect the displacement spectrum and its slope. Higher precision measuring positions of BPs in the NST data appears to be the main reason for the persistent detection of super-diffusion regime in the photosphere.

5. Turbulent Diffusion in Quiet Sun, Coronal Hole and AR Plage Areas

In this section, we discuss the displacement spectra for the CH and ARP data and compare them with the displacement spectrum for the QS data set (Figure 8). Although the three spectra display noticeable difference, they demonstrate that the super-diffusion regime ($\gamma > 1$) is present in all three magnetic areas. In Figure 9, we plot the same spectra in linear coordinates for a short time range only.

The ARP spectrum shows the shallowest slope and smallest displacements, indicating the lowest, among these three samples, level of turbulent diffusion. The CH data show the steepest spectrum and largest displacements. This was expected since BPs in the AR plage area are the most crowded and tightly packed in the narrow inter-granular lanes, when compared to the QS and CH environment (see Figure 1). In the CH, BPs have the most freedom to move, because they have a lower population density. Indeed, from a single CH image, we find the BP surface density to be between 0.08 and 0.65 BP per Mm^2 , while this density is 0.28-0.72 Mm^{-2} and 0.71-1.78 Mm^{-2} in the QS and the AR plage area, respectively. These density values are comparable with those reported in other studies (e.g., Sanchez Almeida et al. 2010). Therefore, turbulent diffusion is most enhanced in a coronal hole on all time scales.

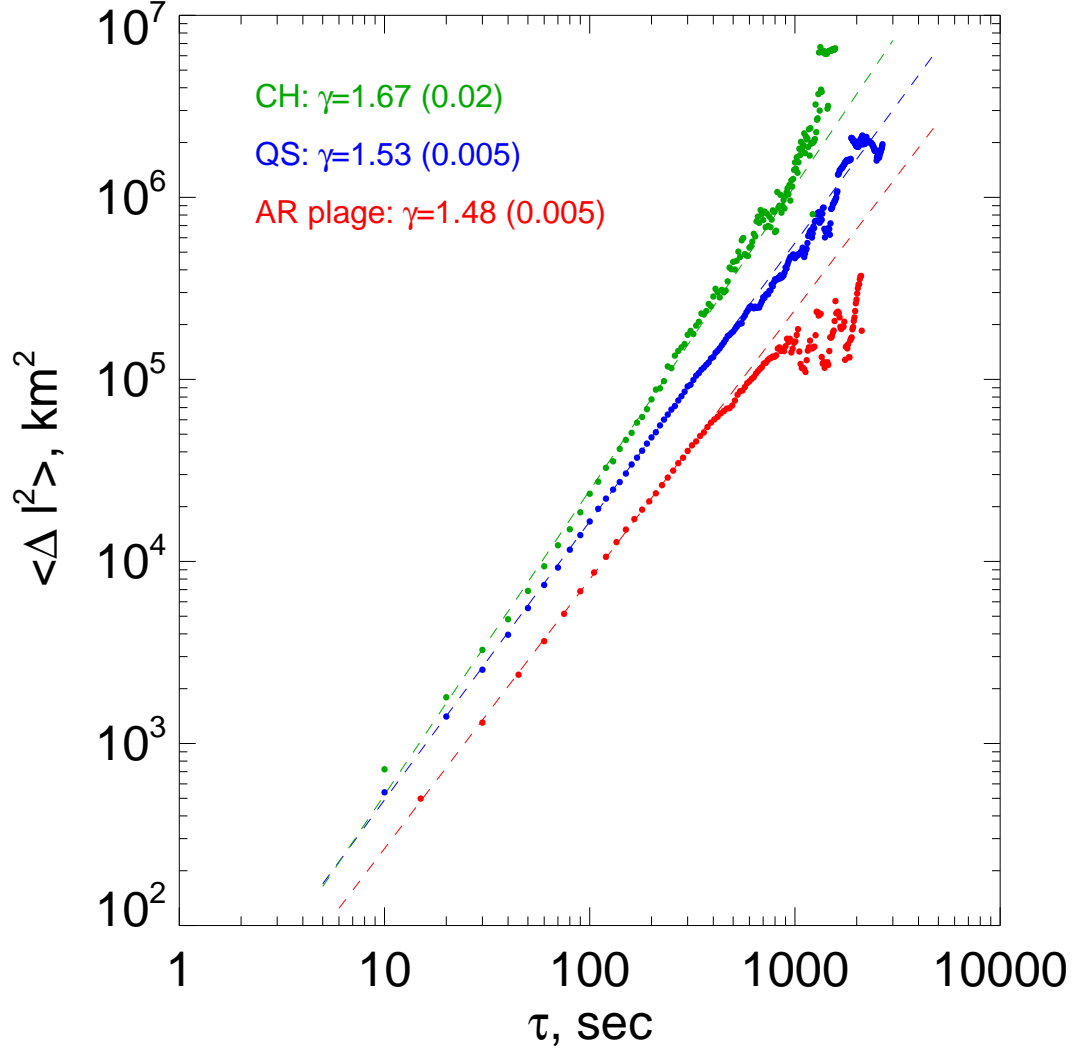


Fig. 8.— Function $(\Delta l)^2(\tau)$ determined for the CH data (green), QS area (blue) and AR plage area (red), according to Eq.1. The error bars do not exceed the size of plotting symbols. Other notations are the same as in Figure 5.

6. Turbulent Diffusion Coefficient as a Function of Scale

Monin & Yaglom (1975) argued that in case of fully developed turbulence, the coefficient of turbulent diffusion of a passive scalar should depend on temporal and spatial scales. In 2D turbulence (in our case - solar surface), the expression for the turbulent

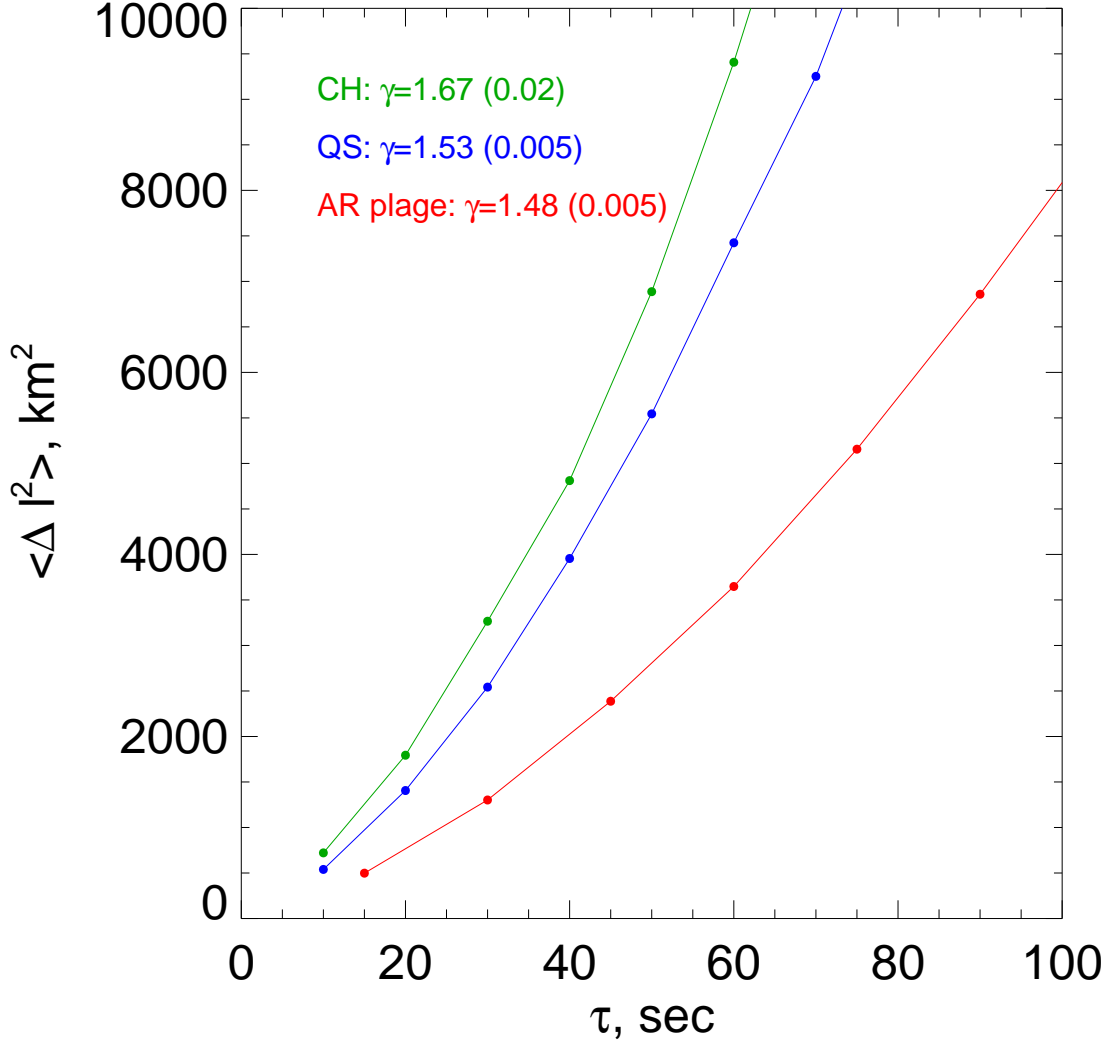


Fig. 9.— The short time scale end of the plot in Figure 8 plotted in linear axes. Notations are the same as in Figure 8.

diffusion coefficient is (see Monin & Yaglom 1975):

$$K(\tau) = \frac{1}{4} \frac{d}{d\tau} \langle l^2(\tau) \rangle, \quad (3)$$

where $\langle l^2(\tau) \rangle$ is a variance of “fluid particle” displacements for given $\tau = t - t_o$. Note that $\langle l^2(\tau) \rangle$ is equivalent to function $(\Delta l)^2(\tau)$, discussed above, which can be approximated, at a

given range of scales (Sections 4 and 5), by

$$(\Delta l)^2(\tau) = c\tau^\gamma, \quad (4)$$

where $c = 10^{y_{sect}}$ and γ and y_{sect} can be derived from the best linear fit to the data points plotted in a double-logarithmic plot. Then the diffusion coefficient can be written as

$$K(\tau) = \frac{c^\gamma}{4}\tau^{\gamma-1}. \quad (5)$$

When τ is excluded from Eqs. 3 and 4, we obtain a relationship between the diffusion coefficient and a spatial scale:

$$K(\Delta l) = \frac{c^\gamma}{4}((\Delta l)^2/c)^{(\gamma-1)/\gamma}. \quad (6)$$

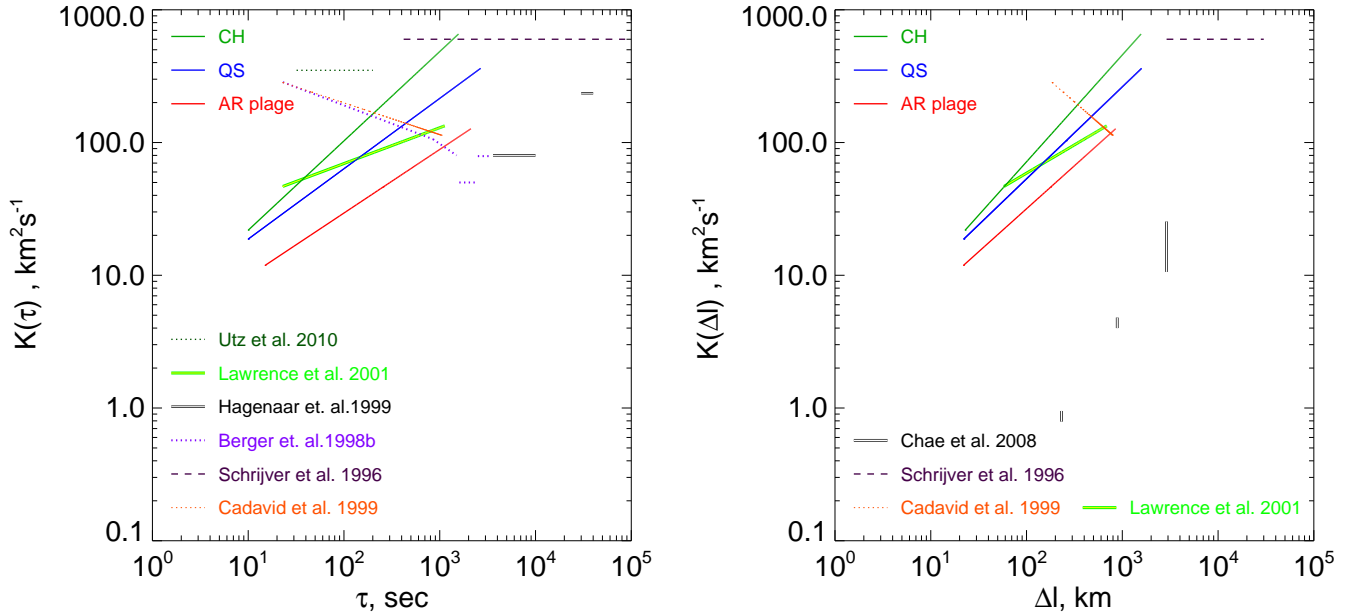


Fig. 10.— Turbulent diffusion coefficient plotted as a function of temporal (left) and spatial (right) scales. Solid lines refer to the NST data shown in Figures 8 and 9 with the same color notations.

Figure 10 (solid lines) plots $K(\tau)$ and $K(\Delta l)$ calculated from the three linear fits presented in Figure 8 by means of Eqs. 5 and 6. The largest diffusion coefficients are measured in the CH, while the smallest ones are detected in the AR plage area, which is in accordance with the strength of the super-diffusion regime in these areas (magnitude of γ). In general, we find that as the temporal and spatial scales decrease, the diffusion coefficient

decreases, too. This holds true only in the case of super-diffusion: indeed, as it follows from Eqs. 5 and 6, for all $\gamma > 1$ both $K(\tau)$ and $K(\Delta l)$ are monotonically increasing functions. When $\gamma = 1$, the diffusion coefficient is constant at all scales (Brownian motion, or random walk), while in the case of sub-diffusion ($\gamma < 1$), the diffusion coefficients decrease with increasing scales.

7. Summary and Discussion

We report the presence of the super-diffusion regime in the displacement of photospheric BPs measured in a quiet-sun area, a coronal hole, and in an active region plage. Super-diffusion, measured by the index γ of the squared displacement spectrum, is weakest in the plage area ($\gamma = 1.48$) and strongest in the coronal hole area ($\gamma = 1.67$). The data quality (spatial resolution, time cadence, alignment) has a direct effect on the result: the better the data quality the more pronounced the super-diffusion regime is. The super-diffusion regime was also detected in the 3D MHD model data of the solar magneto-convection performed by Stein and co-authors (Stein et al. 2007).

We obtained an analytical expression for the turbulent diffusion coefficient as a function of scales and γ . For the case of super-diffusion, the coefficient of turbulent diffusion is directly proportional to both temporal and spatial scales. At the minimal spatial (22 km) and temporal (10 sec) scales considered here the diffusion coefficient in the CH and QS areas was found to be 22 and 19 km² s⁻¹, respectively. Whereas in the AR plage the coefficient was about 12 km² s⁻¹ for the minimal temporal scale of 15 s.

We compare our findings to previous studies of the photospheric diffusion in the quiet sun (see Figure 10).

Hagenaar et al. (1999) tracked magnetic elements using SOHO/MDI high resolution magnetograms and reported a diffusion coefficient increasing with scale (double lines in the left panel of Figure 10).

Chae et al. (2008) determined the diffusion coefficient from observed dynamics of photospheric magnetic fields by solving the equation of magnetic induction. These authors analyzed plage and network areas by utilizing SOHO/MDI full disk and high resolution magnetograms as well as Hinode/SOT data. They reported the smallest magnitudes of K , to date, for three spatial scales (double lines in the right panel of Figure 10). It is worth noting that these three data points are in a very good agreement with both Kolmogorov and Iroshnikov-Kraichnan scaling (see Figure 4 in Chae et al. 2008).

Utz et al. (2010) estimated the diffusion coefficient in the framework of the normal diffusion paradigm, and therefore, their results do not depend on scale (green dots in the left panel of Figure 10). They reported the value of $K = 350 \pm 20 \text{ km}^2 \text{ s}^{-1}$ for the time interval of 32 - 200 s.

Schrijver et al. (1996) reviewed earlier data on the diffusion coefficient and argued that the reported values, which are around $200 \text{ km}^2 \text{ s}^{-1}$, should be multiplied by a factor of 2-3 to account for the high mobility of small (unresolved) magnetic features that may contribute significantly in the resulting diffusivity. The corrected diffusivity of about $600 \text{ km}^2 \text{ s}^{-1}$ (dashed lines in Figure 10) is then in a good agreement with the well-performing model for the magnetic flux transport during a solar cycle (Wang & Sheeley 1994).

Berger et al. (1998b) analyzed a G-band data set obtained with the SVST on October 5, 1995 (the same data set was utilized later in Cadavid et al. 1999 and Lawrence et al. 2001). The authors used a BP tracking method (Löfdahl et al. 1998, Berger et al. 1998a). They found a nearly constant diffusion coefficient of $50 \text{ km}^2 \text{ s}^{-1}$ inside the 1600-2400 s time interval and $79 \text{ km}^2 \text{ s}^{-1}$ inside the 2500-3400 s interval (blue dots in the left panel of Figure 10). For shorter (< 1500 s) time scales, the authors reported a diffusion coefficient decreasing with spatial scale, and they thus concluded that a normal diffusion approximation is not applicable for short time scales.

We also used the displacements spectra shown in Figure 1 of Cadavid et al. (1999) and in Figure 2 of Lawrence et al. (2001) to calculate the diffusion coefficient by means of Eqs. 5 and 6 (the orange dots and the green double line, respectively, in Figure 10). Cadavid et al. (1999) displacements spectrum produced a diffusion coefficient that is inversely proportional to scales (both temporal and spatial), indicating a dominant sub-diffusion regime. Lawrence et al. (2001) displacements spectrum produced a diffusion coefficient that increases with scales, however the rate of increase is slower than that derived from the NST data.

The turbulent diffusion coefficients were derived in this study from the second moment of displacements (see Eqs. 5 and 6). Lawrence et al. (2001) utilized a general expression for the diffusivity index, $\gamma(q)$, treating it as a function of the statistical moment, q :

$$\langle (\Delta l)^q \rangle^{1/q} \sim \tau^{\gamma(q)/2}. \quad (7)$$

These authors found that in the limit of a very large data set, the magnitude of γ tends to be independent of q . Moreover, they showed that errors in calculating of γ become significantly smaller when $q \rightarrow 0$. Therefore, it is useful to derive γ for small q and compare it with that obtained for $q = 2$. From our QS data set, we derived $\gamma(0.1) = 1.580 \pm 0.0035$, which is only 3% higher than $\gamma(2) = 1.530 \pm 0.005$. Note that from the SVST data,

Lawrence et al. (2001) obtained $\gamma(0.1) = 1.27 \pm 0.01$ and $\gamma(2) = 1.13 \pm 0.01$, and they differ from each other by 12%. Moreover, the obtained here magnitude of γ is in a very good agreement with that predicted from the CTRW approach, $\gamma = 1.54$ (Lawrence et al. 2001).

Modern models of the small-scale turbulent dynamo in the photosphere (Boldyrev & Cattaneo 2004; Vögler & Schüssler 2007; Pietarila Graham et al. 2009) utilize the collisional value of magnetic diffusivity ($0.01 - 10 \text{ km}^2\text{s}^{-1}$) based on the electric conductivity in the photosphere. At the same time, utilizing the turbulent magnetic diffusivity would be more justified physically, as long as the turbulent diffusivity determines the minimum scale for magnetic elements. The measured so far value of turbulent magnetic diffusivity ($70\text{-}350 \text{ km}^2\text{s}^{-1}$), being interpreted as a scale-independent parameter, leaves a very slim chance to successfully model the small-scale turbulent dynamo in the photosphere. Thus, in the case of very high diffusivity on very small scales (sub-diffusivity), chances for tiny magnetic field concentrations to resist the spreading action of turbulent flows are small, so that the dynamo is restrained. A super-diffusion regime on very small scales is very favorable for pictures assuming the turbulent dynamo action since it assumes decreasing diffusivity with decreasing scales. The idea of a small-scale turbulent dynamo operating in the quiet sun photosphere received strong observational support when turbulent magnetic fields were discovered with Hinode instruments (Centeno et al. 2007; Lites et al. 2008; Orozco Suarez et al. 2008; Schüssler & Vögler 2008).

Author are thankful to BBSO instrument team and observers for their contribution to data acquisition. We are obliged to the anonymous referee whose comments helped much in improving the manuscript. VA work was partially supported by NSF grant ATM-0716512. VY acknowledges support from NASAs GI NNX08AJ20G and LWS TR&T NNG0-5GN34G grants. PG, VA and VY are partially supported by NSF (AGS-0745744), NASA (NNY 08BA22G) grants. PG is partially supported by AFOSR (FA9550-09-1-0655). RFS was partially supported by NASA grants NNX07AH79G and NNX08AH44G and NSF grant AST0605738. The simulations were performed on the Pleiades supercomputer of the NASA Advanced Supercomputing Division.

REFERENCES

- Abramenko, V., Yurchyshyn, V., Goode, P.R., Kilcik, A. 2010, ApJ, 725, L1.
- van Ballegoijen, A. A., Nisenson, P., Noyes, R. W., Lofdahl, M. G., Stein, R. F., Nordlund, A., Krishnakumar, V. 1998, ApJ, 509, 435
- Berger, T. E., Löfdahl, M. G., Shine, R. S., Title, A. M. 1998a, ApJ, 495, 973

- Berger, T. E., Löfdahl, M. G., Shine, R. A., Title, A. M. 1998b, *ApJ*, 506, 439
- Berger, T.E., Title, A.M. 2001, *ApJ*, 533, 449
- Barthol, P., Gandorfer, A., Solanki, S. K., Schssler, M., Chares, B., and 40 co-authors, 2011, *Solar Phys.* 268, 1
- Boldyrev, S., Cattaneo, F. 2004, *Phys. Rev. Lett.*, 92, 144501
- Bonet, J. A., Mrquez, I., Snchez Almeida, J., Palacios, J., Martinez Pillet, V., Solanki, S. K., del Toro Iniesta, J. C., Domingo, V., Berkefeld, T., Schmidt, W., Gandorfer, A., Barthol, P., Knlker, M. 2010, *ApJ*, 723, L139
- Cadavid, A.C., Lawrence, J.K., Ruzmaikin, A.A. 1999, *ApJ*, 521, 844
- Campos, D., Mandez, V. 2008, *J. Phys.A: Math. Theor.*, 41, 085101
- Chae, J., Litvinenko, Yu., Sakurai, T. 2008, *ApL*, 683, 1153
- Centeno, R., Socas-Navarro, H., Lites, B., Kubo, M., Frank, Z., and 9 co-authors, 2007, *ApJ*, 666, L137.
- Cranmer, S. R., van Ballegooijen, A. A. 2005, *ApJS*, 156, 265
- Crockett, P. J., Mathioudakis, M., Jess, D. B., Shelyag, S., Keenan, F. P., Christian, D. J., 2010, *ApJ*, 722, L188
- Goode, P. R., Coulter, R., Gorceix, N., Yurchyshyn, V., Cao, W. 2010a, *Astronomische Nachrichten*, 331, 620
- Goode, P. R., Yurchyshyn, V., Cao, W., Abramenko, V., Andic, A., Ahn, K., Chae, J., 2010b, *ApJ*, 714, L31
- Hagenaar, H. J., Schrijver, C. J., Title, A. M., Shine, R. A. 1999, *ApJ*, 511, 932
- Ishikawa, R., Tsuneta, S., Kitakoshi, Y., and 6 co-authors, 2007, *Astronomy and Astrophysics*, 472, 911
- Ishikawa, R., Tsuneta, S. 2010, *ApL*, 718, L171
- Ishikawa, Ryohko; Tsuneta, Saku; Jurčák, Jan 2010, *ApJ* 713, 1310
- Kosugi, T., Matsuzaki, K., Sakao, T., and 22 co-authors, 2007, *Solar Physics*, 243, 3

- Lagg, A.; Solanki, S. K.; Riethmiller, T. L.; Martinez Pillet, V.; Schüssler, M.; and 12 co-authors, 2010, *ApJ*, 723, L164
- Lawrence, J.K., Schrijver, C.J. 1993, *ApJ*, 411, 412
- Lawrence, J. K., Cadavid, A. C., Ruzmaikin, A., Berger, T. E. 2001, *Phys. Rev. Lett.*, 86, Issue 26, 5894
- Lites, B. W., Kubo, M., Socas-Navarro, H., and 11 co-authors, 2008, *ApJ*, 672, 1237
- Löfdahl, M. G., Berger, T. E., Shine, R. S., Title, A. M. 1998, *ApJ*, 495, 965
- Martinez Pillet, V., Del Toro Iniesta, J. C., Ivaréz-Herrero, A., Domingo, V., Bonet, J. A., and 37 co-authors, 2011, *Solar Physics*, 268, 57
- Monin, A.S. & Yaglom, A.M. 1975, *Statistical Fluid Mechanics*, ed. J.Lumley (MIT Press, Cambridge, MA)
- Muller, R., Dollfus, A., Montagne, M., Moity, J., Vigneau, J. 2000, *Astronomy and Astrophysics*, 359, 373
- Orozco Suarez, D., Bellot Rubio, L. R., del Toro Iniesta, J. C., Tsuneta, S. 2008, *Astron. Astrophys.* 481, L33
- Pietarila Graham, J., Danilovic, S., Schüssler, M. 2009, *ApJ*, 693, 1728
- Petrovay, K. 2001, *Space Science Reviews*, 95, 9
- Pietarila Graham, J., Cameron, R., Schüssler, M. 2010, *ApJ*, 714, 1606
- Sánchez Almeida, J., Bonet, J. A., Viticchi, B., Del Moro, D. 2010, *ApJ*, 715, L26
- Scharmer, G.B., Dettori, P., Löfdahl, M.G., Shand, M. 2003, in *Innovative Telescopes and Instrumentation for Solar Physics*, ed. S. Keil and S. Avakyan, *Proc SPIE*, 4854, 341
- Scherrer, P. H., Bogart, R. S., Bush, R. I., Hoeksema, J. T., Kosovichev, A. G., Schou, J., Rosenberg, W., Springer, L., Tarbell, T. D., Title, A., Wolfson, C. J., Zayer, I., MDI Engineering Team, 1995, *Solar Physics*, 162, 129
- Schrijver, C. J., Shine, R. A., Hagenaar, H. J., Hurlburt, N. E., Title, A. M., Strous, L. H., Jefferies, S.t. M., Jones, A. R., Harvey, J. W., Duvall, T. L., Jr. 1996, *ApJ*, 468, 921
- Schüssler, M., Vögler, A. 2008, *Astron Astrophys.* 481, L5

- Stein, R. F., Benson, D., Nordlund, A. 2007, in: *New Solar Physics with Solar-B Mission ASP Conference Series*, Vol. 369, proceedings of the conference held 8-11 November, 2005 at The Kyoto International Community House, Kyoto, Japan. Edited by Kazunari Shibata, Shin'ichi Nagata, Takashi Sakurai. San Francisco: Astronomical Society of the Pacific, 2007., p.87
- Title, A. M.; Tarbell, T. D.; Topka, K. P.; Ferguson, S. H.; Shine, R. A.; SOUP Team, 1989, *ApJ*, 336, 475.
- Tsuneta, S., Ichimoto, K., Katsukawa, Y., and 22 co-authors, 2008, *Solar Phys.*, 249, 167
- Utz, D., Hanslmeier, A., Mostl, C., Muller, R., Veronig, A., Muthsam, H. 2009, *Astronomy and Astrophysics*, 498, 289
- Utz, D., Hanslmeier, A., Muller, R., Veronig, A., Rybak, J., Muthsam, H. 2010, *Astron Astrophys.* 511, A39
- Vögler, A., Schüssler, M. 2007, *Astron Astrophys*, 465, L43
- de Wijn, A. G., Lites, B. W., Berger, T. E., Frank, Z. A., Tarbell, T. D., Ishikawa, R. 2008, *ApJ*, 648, 1469
- de Wijn, A. G., Stenflo, J. O., Solanki, S. K., Tsuneta, S. 2009, *Space Science Reviews*, 144, 275
- Wang, Y.-M., Sheeley, N. R., Jr. 1994, *ApJ*, 430, 399
- Wöger, F., von der Lühe, O., Reardon, K. 2008, *A& A*, 488, 375
- Zoia, A., Nel, M.C., Cortis, A. 2010, *Phys. Rev. E*, 81, 031104